Towards Industrial Solar Production of Zinc and Hydrogen – Modeling and Design of a 100 kW Solar Pilot Reactor for ZnO Dissociation

D. Gstoehl, T. Cooper, W. Villasmil, A. Meier

This document appeared in

Detlef Stolten, Thomas Grube (Eds.):
18th World Hydrogen Energy Conference 2010 - WHEC 2010
Parallel Sessions Book 2: Hydrogen Production Technologies – Part 1
Proceedings of the WHEC, May 16.-21. 2010, Essen
Schriften des Forschungszentrums Jülich / Energy & Environment, Vol. 78-2
Institute of Energy Research - Fuel Cells (IEF-3)
Forschungszentrum Jülich GmbH, Zentralbibliothek, Verlag, 2010
ISBN: 978-3-89336-652-1

Towards Industrial Solar Production of Zinc and Hydrogen – Modeling and Design of a 100 kW Solar Pilot Reactor for ZnO Dissociation

D. Gstoehl, T. Cooper, W. Villasmil, A. Meier, Paul Scherrer Institut, Solar Technology Laboratory, 5232 Villigen PSI, Switzerland

A two-step water-splitting thermochemical cycle based on the Zn/ZnO redox reactions is proposed for producing solar hydrogen; the two steps are (1) the endothermal dissociation of ZnO and (2) the exothermal reaction of H_2O with Zn to produce hydrogen. A preliminary engineering design of a 100 kW solar pilot reactor for the thermal dissociation of ZnO is presented. The reactor features a rotating cavity receiver lined with ZnO particles. With this arrangement, ZnO is directly exposed to concentrated solar radiation and serves simultaneously the functions of radiant absorber, chemical reactant, and thermal insulator. The functionality of the engineering design has earlier been demonstrated with a 10 kW reactor prototype at temperatures above 2000 K and peak solar concentration ratios exceeding 4000 suns. The solar chemical reactor, depicted in Fig. 1, is described in detail in a previous publication [1]. Here, we present a brief summary of the main features. The rotating cylindrical cavity is made of sintered Al_2O_3 tiles placed on top of a multi-layer Al_2O_3-SiO_2-Y_2O_3-based ceramics for thermal shock resistance, mechanical stability, gas diffusion barrier, and thermal insulation. Along the horizontal axis, a dynamic feeder extends and contracts within the rotating cylindrical cavity, forming a layer of ZnO particles along the cavity walls. The directly irradiated ZnO(s) is thermally decomposed, and the gaseous products Zn(g) and O_2 exit the cavity through a water-cooled annular gap between the outlet tube and the feeder. Inert Ar gas is injected for aerodynamic window protection and for minimizing recombination of product gases of Zn(g) and O_2 to ZnO(s) in the cavity.

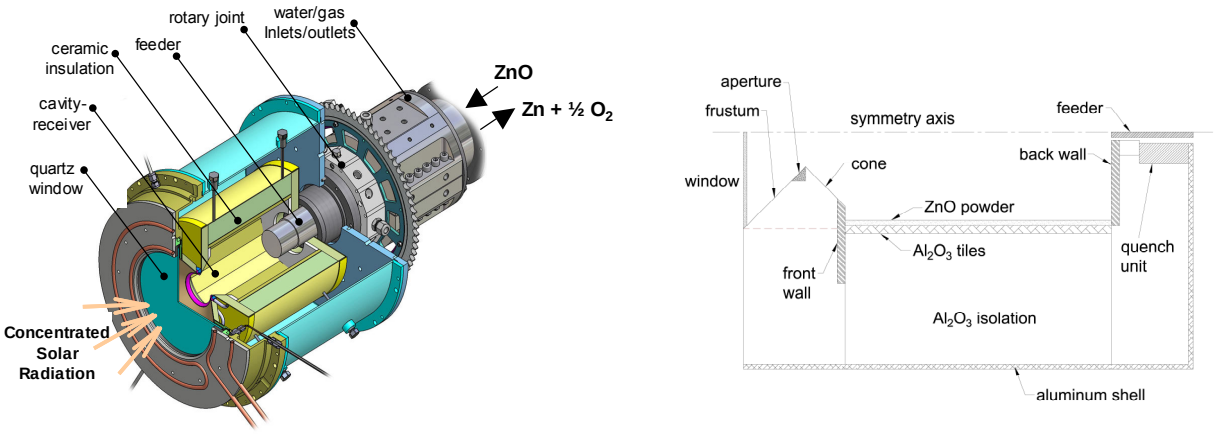

Figure 1: ***Left:*** **Schematic of the solar chemical reactor configuration. From [1].** ***Right:*** **Scheme of the reactor geometrical domain used for the numerical model.**

The planned test site for the 100 kW scale-up reactor is the Megawatt Solar Furnace (MWSF) at the Laboratoire PROcédés, Matériaux et Energie Solaire (PROMES) research facility in Odeillo, France [2].

The MWSF consists of a south-facing field of 63 flat heliostats (7.5 m x 6 m), a north-facing parabolic concentrator dish (height 40 m, width 54 m) , and a receiver tower (height 20 m) arranged as shown in Fig. 2. The heliostats are elevated on a series of eight stepped terraces such that the reflected beam from each heliostat is parallel to the axis of revolution of the parabolic dish. Each terrace contains two rows of heliostats such that, at moderate tilt angles, no horizontal gaps exist between heliostats as projected onto the parabolic dish. Additionally, the elevations of the terraces are arranged in a manner such that (again at moderate tilt angles) no vertical gaps exist between heliostats as projected onto the parabolic dish. Optical and geometric data of the site − receiver tower, heliostats and parabolic dish – were obtained from [2]. For the intended size of the scale-up reactor, the full capacity of the MWSF is not required. The 25 center heliostats will likely be sufficient to achieve the necessary power input of 100 kW. The subsequent analysis is therefore limited to these 25 heliostats of interest.

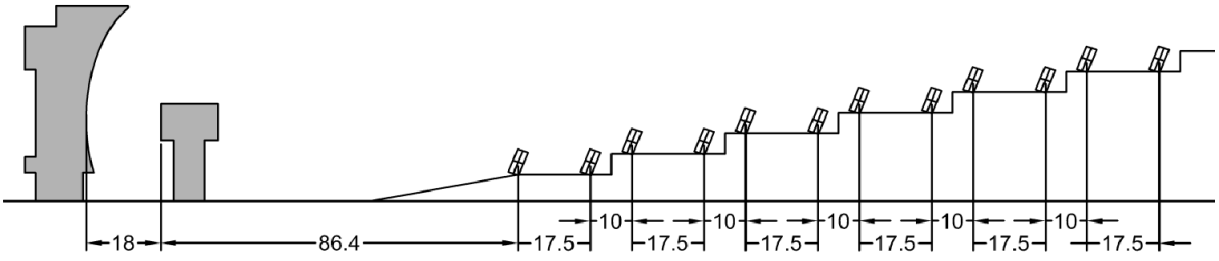

Figure 2: Side elevation of the MWSF showing distances in meters from the focal plane to the vertex of the parabolic dish and to each row of heliostats for the 25 heliostats of interest. Data provided by CNRS-PROMES.

An in-house Monte Carlo (MC) ray-tracing code VeGaS [3] has been adapted to the geometry of the MWSF with the goal of estimating the flux distribution within the scale-up reactor [4]. Parameter matching was performed to obtain close agreement between the MC ray-tracing results and the experimentally derived curve of incident solar flux for a flat target positioned at the focus [4]. Three parameters – the fraction of diffuse reflection, f_{diff}, and the angular dispersion error of the heliostats, $\phi_{err,helio}$, and parabolic dish, $\phi_{,err,PD}$ – were considered. The angular dispersion error includes the combined effect of macroscopic geometric imperfections and heliostat tracking errors. The fraction of diffuse reflection includes the combined effect of microscopic imperfections, such as surface roughness, and the degradation of surface reflectivity from dust and atmospheric exposure. The best fit parameter match yielded a total combined dispersion error of 6 mrad, split evenly between heliostats and parabolic dish ($\phi_{err,helio}$ = $\phi_{,err,PD}$ = 3 mrad) and a fraction of diffuse reflection of f_{diff} = 0.05 for the mirror surfaces. A comparison of the simulated and experimentally measured flux distribution on the flat target is given in Fig. 3.

A transient heat transfer model was adapted to simulate the thermal performance of the 100 kW pilot reactor for the solar-driven dissociation of ZnO at MWSF [5]. The model couples radiation, convection, and conduction heat transfer to the reaction kinetics for a shrinking domain and simulates a transient ablation regime with semi-batch feed cycles of ZnO particles. Experimental model validation was previously accomplished with a 10 kW reactor prototype in terms of temperatures and reaction extents [6].

Geometric dimensions used for the preliminary 100 kW reactor design are listed in Table 1 [6]. The porosity and the extinction coefficient of the ZnO layer have been taken as 0.5 and 7850 m^{-1}, respectively. In the proposed design, the cavity, as well as the back and front walls are assumed to be covered with a 40 mm thick sintered ZnO layer followed by 10 mm thick Al_2O_3 tiles. The function of the ZnO layer is to protect the Al_2O_3 tiles from the highly radiative environment. The power distribution obtained from the ray-tracing was scaled such that 100 kW input power is effectively absorbed within the reactor cavity.

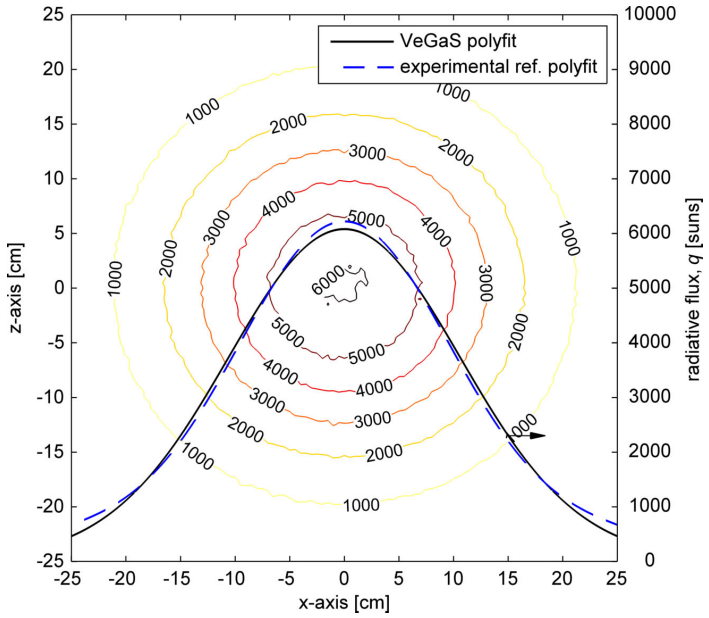

Figure 3: Contour map of incident radiative flux for a flat target at the focus of the parabolic dish comparing the parameter-matched VeGaS simulation ($\phi_{err,helio} = \phi_{,err,PD} = 3$ mrad; $f_{diff,helio} = f_{diff,PD} = 0.05$) to the experimentally measured distribution. Results are for a direct normal solar irradiance of 1 sun (1 sun = 1000 W/m^2) for a solar altitude angle of 45° at solar noon. Experimental data provided by CNRS-PROMES.

Table 1: Dimensions for the 100 kW pilot reactor as proposed by [6].

Cavity diameter	500	mm
Cavity length	750	mm
Sintered ZnO layer thickness	40	mm
Al_2O_3 tiles thickness	10	mm
Outer Al shell diameter	110	mm
Aperture diameter	190	mm
Window diameter	370	mm
Cavity outlet diameter	80	mm
Frustum angle	45	deg

The radiative flux distribution within the 100 kW reactor at the MWSF is illustrated in Fig. 4. Highest concentrations are obtained on the bottom part of the cavity cylinder and on the frustum. Nearly 90% of the radiative power that enters the aperture is absorbed on the cavity cylindrical wall, while the rest is mostly absorbed by the lateral back wall and the cone. Only 0.1% of the incoming solar radiation is lost through the back exit of the reactor by direct transmission or reflection. In the experimental runs, the rotary motion of the cavity effectively averages the radiative flux distribution along the circumference of the cylinder.

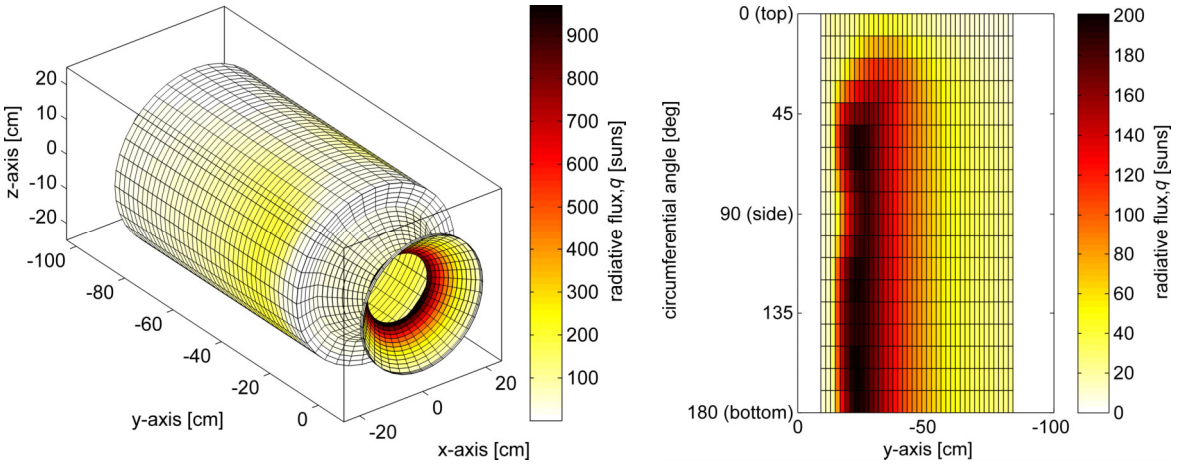

Figure 4: Radiative flux distribution on the reactor (*left*) and on the cylindrical cavity surface (*right*). Note that the radiative flux on the internal cavity walls is much less than on the frustum due to the distribution of the incident radiation over a much larger surface area within the cavity. 1 sun = 1000 W/m^2.

The 100 kW reactor was simulated for two consecutive days of operation. For the first day, the incoming radiative power is increased linearly from zero to the nominal power over a 1-hour time span to avoid overheating of the reactor components. The power is then held constant for 8 hours, followed by 15 hours of zero incident power, simulating the operation overnight when no solar radiation is available. The second day was modeled in a similar way, the only difference being that no time span was considered for heating up of the reactor as it would still preserve an important portion of the sensible heat accumulated during the previous day.

Figure 5 (left) shows the predicted temperatures at the sintered-ZnO surface and at the Al_2O_3-tile surface halfway along the cavity cylinder. The model results indicate that temperatures above 2000 K are likely to be reached at the sintered-ZnO surface. To avoid failure of the Al_2O_3 tiles at such high temperatures, a protecting layer of sintered ZnO is required on the cylindrical cavity walls as well as on the lateral front and back walls. With the proposed ZnO layer thickness of 40 mm, the maximum surface temperature of the Al_2O_3 tiles is not expected to exceed 1900 K.

The predicted reactor performance is illustrated graphically in Fig. 5 (right) and summarized in Table 2. The amount of ZnO dissociated is expected to be approximately 250 kg per day, corresponding to an average dissociation rate of about 8 g/s. The solar-to-chemical energy conversion efficiency, $\eta_{\text{solar-to-chemical}}$, is defined as

$$\eta_{solar \rightarrow chemical} = \frac{r\left(\Delta H_r(T) + \int_{T_0}^{T} c_{p,ZnO}\, dt\right)}{Q_{solar}}$$

where ΔH_r is the reaction enthalpy, c_p is the specific heat capacity, and Q_{solar} is the solar power absorbed by the cavity (100 kW). In contrast, the reactor efficiency, $\eta_{reactor}$, and the shares of the radiation, conduction, and convection losses presented in Table 2, have been calculated based on the total incident radiative power on the reactor window (190 kW). 10% of the incoming solar radiation is expected to be lost at the window due to reflections at its outer surface. The simulation anticipates the reradiation losses to account for approximately 40% of the total incident power on the window. The water-cooled components − namely, the quench unit, the reactor front shield and the aperture ring − were modeled at 298 K. As approximately 7% of the total incident radiative power is absorbed by the aperture ring, the heat loss associated to this component represents by far the highest share of the conduction losses.

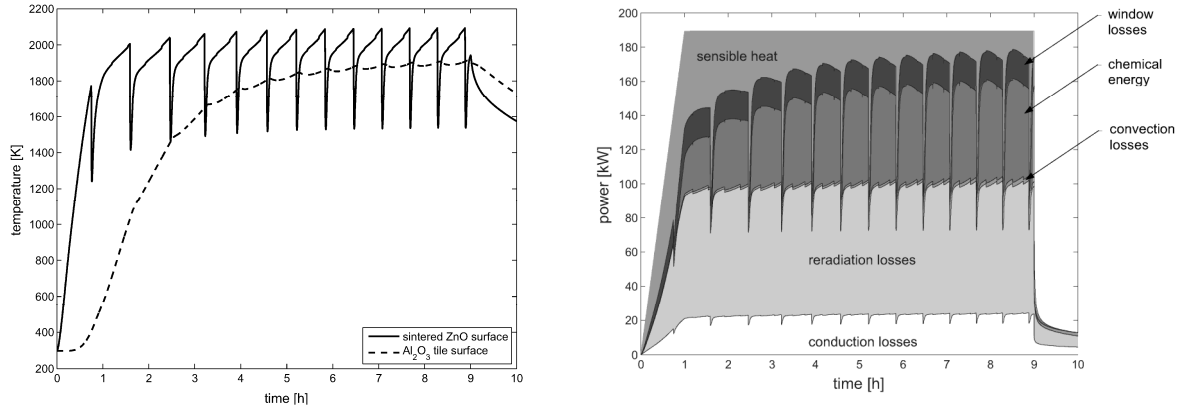

Figure 5: ***Left:*** **Predicted temperatures halfway along the cavity of the 100 kW ZnO dissociation reactor, both at the sintered-ZnO surface and at the Al_2O_3-tile surface.** ***Right:*** **Instant energy balance of the 100 kW ZnO dissociation reactor as it would operate at the Odeillo solar furnace. The concentrating solar system configuration is such that 100 kW input power is effectively absorbed within the reactor cavity.**

Since for the second day of operation less energy is required to heat up the reactor components, the average bulk reactor temperature is predicted to be higher for the second day, resulting in a higher dissociation rate and higher efficiencies. Scaling up the reactor to 100 kW solar thermal power input has thus the potential of reaching solar-to-chemical energy conversion efficiencies approaching 50%.

Table 2: Predicted energy balance for the 100 kW pilot reactor.

	Day 1	Day 2	
Reaction rate	26	30	kg/h
$\eta_{solar\text{-}to\text{-}chemical}$	42.4	46.2	%
$\eta_{reactor}$	22.3	24.2	%
Reradiation losses	40.6	40.9	%
Conduction losses	14.6	14.8	%
Convection losses	2.4	3.1	%
Sensible heat of the reactor	10.1	7.0	%
Window losses	10.0	10.0	%

Acknowledgments

Financial support by the Swiss Federal Office of Energy (SFOE) is gratefully acknowledged. We thank CNRS-PROMES for the collaboration, especially E. Guillot and J.-L. Sans for providing information concerning the MWSF. We are grateful to M. Hänchen and P. Coray for fruitful discussions and computational support.

References

[1] L.O. Schunk, P. Haeberling, S. Wepf, D. Wuillemin, A. Meier, A. Steinfeld: ***A receiver-reactor for the solar thermal dissociation of zinc oxide****, J. Solar Energy Eng.* 130 (2), 021009, 2008.

[2] CNRS-PROMES: "CNRS 1000 kW solar furnace," Centre National de la Recherche Scientifique (CNRS), 2010, http://www.promes.cnrs.fr/TOUT-PUBLIC/Les-fours/eng-lesfours1.htm

[3] J. Petrasch: ***Thermal modeling of solar chemical reactors: transient behavior, radiative transfer***, MS Thesis, ETH Zürich, 2002.

[4] T. Cooper: ***Ray-tracing analysis of a concentrating solar facility for the optical design of solar cavity receivers***, MS Thesis, ETH Zürich, 2010.

[5] W. Villasmil: ***Design of a 100-kW reactor for the solar thermal dissociation of zinc oxide***, MS Thesis, ETH Zürich, 2010.

[6] L.O. Schunk, W. Lipiński, A. Steinfeld: ***Heat transfer analysis of a solar receiver-reactor for the thermal dissociation of ZnO – Experimental validation at 10 kW and scale-up to 1 MW****, Chem. Eng. J.* 150, pp. 502-508, 2009.